Advances in Renewable Energies Offshore – Guedes Soares (Ed.)

Estimating the offshore wind energy along the Portuguese coast using WRF and satellite data

N. Salvação
Centre for Marine Technology and Ocean Engineering (CENTEC), Instituto Superior Técnico, Universidade de Lisboa, Lisbon, Portugal

A. Bentamy
Institut Français de Recherche pour l'Exploitation de la MER (IFREMER), Brest, France

C. Guedes Soares
Centre for Marine Technology and Ocean Engineering (CENTEC), Instituto Superior Técnico, Universidade de Lisboa, Lisbon, Portugal

ABSTRACT: The wind energy offshore the Portuguese coast is estimated using two wind datasets: the output from numerical model WRF and a wide array of satellite data. To determine the inherent errors of the two sources, the wind data is firstly validated with in situ measurements obtained from marine buoys moored along the Iberian Peninsula Coast. Additionally, the potential benefit of blending the two sets of data to create a high resolution wind data set is investigated. The energy available for conversion by wind turbines is estimated over the entire domain with special focus on 8 proposed locations for the construction of wind parks. The results show that the use of multi-satellite information can improve the wind speed predictions, reducing the uncertainty of wind energy estimates. Despite the similarity of the mean wind speed projections from the two data sources, the differences achieved when computing the available energy cannot be disregarded.

1 INTRODUCTION

The increasing interest in renewable energy systems reflects the urgent need for a sustainable development of the planet. More specifically, the European Union has settled ambitious targets for climate action and energy efficiency, promoting the scientific research and innovation on these topics (European Commission, 2015). The wind soon drew the attention of the industry, mostly for being the world's second largest source of clean and efficient energy. The lower number of government and environmental constraints offshore, motivated the expansion of the marine energy industry (Stolpe et al., 2014). However, to ensure the cost-effectiveness of a project, a thorough accounting of all the constraints that might be associated to the construction of offshore facilities is necessary (Castro-Santos et al. 2016).

It is important to develop tools for the wind community to be able to plan future use of available resources and manage operation and maintenance activities, which can represent up to 30% of the project lifetime cost (Martin et al., 2016). Simultaneously, the collection of high spatial and temporal resolution wind data at different heights is indispensable.

Typical methodologies for the identification of sustainable offshore wind resources at a candidate area make use of wind measurements obtained from on-site or nearby weather stations such as meteorological masts equipped with wind vanes and anemometers (Soler-Bientz et al., 2010; Lee et al., 2013). However, the use of this data has several limitations. Meteorological masts are very expensive, often sparsely located and not available where the measurements are most needed. Nevertheless this equipment can measure winds at different locations and altitudes, a key element for detailed wind sensing at the hub height of modern wind turbines.

An alternative method to wind masts is the use of remote sensing instruments. Satellite data has been widely used for building offshore wind climatology maps in recent years showing promising results. The results are particularly encouraging when data from multi satellites is used, either alone or when combined with other sources of information (Wei et al., 2018; Guo et al., 2018; Chang et al., 2015 Campos & Guedes Soares, 2017).

Numerical models have also been popular choices as far as wind mapping is concerned. These tools can provide weather information at both short and long time ranges, at high spatial and temporal resolutions (Salvação et al., 2014; Mattar & Borvarán, 2016; Salvação & Guedes Soares, 2016). They represent a clear advantage at sites where information is scarce, such as remote environments and offshore regions. However, there is a high level of uncertainty regarding numerical model results, which prompted numerous attempts for its quantification (Cardinali et al., 2014; Moosavi et al., 2018).

The skill of the simulations is intrinsically bound to the quality of lateral boundary conditions as well as the ability of the chosen physic formulations to describe the short scale atmospheric motions over a particular region. Combining deterministic models with observations from reliable sources will therefore provide a direction for error correction and uncertainty estimation (Hölbig et al., 2016). Previous studies have already demonstrated the potential benefit of using satellite data for building trustworthy wind maps (Salvação et al., 2015). But despite the unquestionable better quality of the satellite data when compared with numerical model predictions, a merged or reconstructed product has a better spatial and temporal coverage (Chang et al., 2015).

In this context, this study provides a comparison between the energy estimates obtained using winds from the numerical model WRF and data retrieved from multiple satellite systems. The data is firstly validated for a quality assessment, using weather information obtained from a network of buoys located along the Portuguese and Spanish coasts. The strengths and weaknesses of the two sources of data are identified, further providing guidance on how to correct the deficiencies encountered. Energy estimates derived from the two datasets are compared in detail with particular focus on 8 proposed areas for the construction of wind parks. The work provides guidance for a trustworthy wind resource assessment, combining the benefits of model and satellite data.

2 DESCRIPTION OF THE WIND DATA

2.1 *WRF model*

The Weather Research and Forecast model (WRF) is one of the most widely used mesoscale models, mostly due to its proficient forecasting and atmospheric research capabilities, suitable for numerous applications. It features multiple dynamical cores, a data assimilation system, a broad spectrum of physics and dynamics options and a software architecture that allows high performance computing. A detailed description of the model can be found in Wang et al. (2018).

The model is configured here to downscale the Era-Interim reanalysis data with 0.25 degrees of horizontal resolution to an approximately 9 km grid spacing mesh. Figure 1 shows the operational set-up of the WRF system. The model has previously been used to map the energy resources for the recent decade, providing realistic projections at potential installation sites (Salvação et al., 2018). In this study, for the validation and creation of the wind maps, the year of 2013 was chosen as a representative of the past decade. The parameterization schemes selected and the WRF options outlined in Table 1 have been carefully selected and formerly validated.

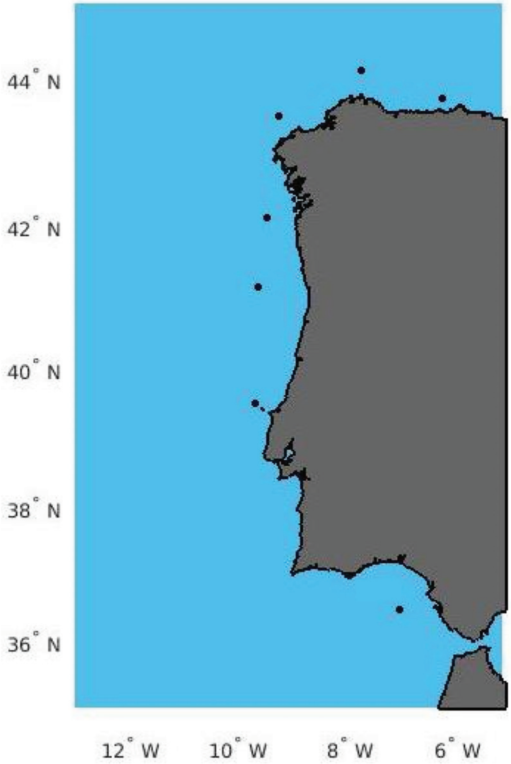

Figure 1. WRF domain and location of the offshore buoys from EMODNET database.

Table 1. Description of the computational grids and parameterization options of the WRF model.

Horizontal resolution (km)	9
Grid Dimension	96 × 148
Vertical Grid dimension	47 eta levels
Radiation	CAM scheme for both short and long wave radiation
PBL Physics	Yonsei University scheme
Land Surface	Unified Noah Land Surface Model
Microphysics	WRF Single-Moment 6-class scheme
Cumulus	Kain-Fritsch scheme

2.2 *Multi-satellite wind data*

This section describes the characteristics of the remotely Sensed Wind Observations used for energy calculations. The data was retrieved from various radars and radiometers onboard satellites and interpolated onto the WRF grid with approximately 0.09 degrees in latitude and longitude spacing. Surface wind speed information has been available from scatterometers, Synthetic-aperture radar, passive microwave imagers and altimeters. They include: two scatterometers onboard the European Remote Sensing Satellites ERS-1 and ERS-2, operated by the European Space Agency (ESA); NASA's active Ku-band scatterometer (NSCAT) launched aboard the Japanese Advanced Earth Observing Satellite (ADEOS-1); SeaWinds scatterometer onboard QuikSCAT satellite; SeaWinds scatterometer onboard the ADEOS II spacecraft; Advanced SCATterometer ASCAT-A and ASCAT-B onboard METOP-A and -B satellites; Oceansat-2 Scatterometer (OSCAT); RapidScat onboard the International Space Station (ISS); Special Sensor Microwave Imager (SSM/I) on board Defense Meteorological Satellite Program (DMSP) F10, F11, F12, F13, F14, and F15, F16, F17, and F18 satellites; JASON1, and JASON2 satellites; Sentinel-1 A's SAR radar instrument; TOPEX/Poseidon Altimetry data and radiometer WindSat onboard CORIOLIS satellite. Table 2 provides a summary of the satellite data specifications and operating periods.

Table 2. Summary of the satellite winds source and operating period.

Satellite	Type of instrument	Period
ERS-1	Scatterometer	1992–1996
ERS-2		1995–2001
NSCAT		1996–1997
QuikSCAT		1999–2009
ASCAT-A		2007–Present
ASCAT-B		2012–Present
OSCAT		2009–2014
SeaWinds		2002–2003
Rscat		2014–2016
Sscat		2016–Present
SENTINEL 1 A	SAR	2014–Present
Topex/Poseidon	altimeter	1992–2005
Jason1		2001–2013
Jason2		2008–Present
SSMI-f10	Radiometer	1992–1997
SSMI-f11		1992–2000
SSMI-f13		1995–2009
SSMI-f14		1997–2008
SSMI-f15		1999–2006
SSMI-f16		2003–Present
SSMI-f17		2006–Present
SSMI-f18		2009–Present
amsre		2002–2011
amsr2		2012–Present
windsat		2003–Present

3 VALIDATION AND ANALYSIS OF NEAR SURFACE WIND SPEEDS

3.1 *Statistical analysis*

This section provides a brief description of the quality check performed for the two wind datasets, by means of a statistical analysis of four scores. The evaluation is performed computing the average values of bias, root mean square error (RMSE), Mean absolute error (MAE) and Pearson's Correlation Coefficient (r). The proposed metrics provide an overall appreciation of the ability of both datasets in replicating the measured wind conditions. They are defined by:

$$Bias = \frac{\sum_{i=1}^{n}\left(X_i - Y_i\right)}{n} \tag{1}$$

$$r = \frac{\sum_{i=1}^{n}\left(X_i - \tilde{X}\right)\left(Y_i - \tilde{Y}\right)}{\left(\sum_{i=1}^{n}\left(X_i - \tilde{X}\right)^2 \sum_{i=1}^{n}\left(Y_i - \tilde{Y}\right)^2\right)^{1/2}} \tag{2}$$

$$RMSE = \sqrt{\frac{\sum_{i=1}^{n}\left(X_i - Y_i\right)^2}{n}} \tag{3}$$

$$MAE = \frac{1}{n}\sum_{i=1}^{n}\left|X_i - Y_i\right| \tag{4}$$

where Y_i represents the measured values, X_i the simulated or satellite values, $\tilde{Y}$ is the mean of the measured values, $\tilde{X}$ is the mean of the simulated values, and n is the number of observations.

Each time series is compared against 1-hourly wind measurements obtained from a network of 7 marine buoys. The location of the stations is represented in Figure 1. The marine buoy data was obtained from the EMODNET database (http://www.emodnet.eu/) and provides wind data at 3 m height. For this reason, the wind is adjusted to 10 m using the logarithmic wind profile expression:

$$u_z = u_{zm} \times \ln\left(\frac{z}{z_0}\right) / \ln\left(\frac{z_m}{z_0}\right) \tag{5}$$

where u_{zm} is the known wind speed at a reference height z_m, and z_0 is the roughness length. Assuming a neutrally stable atmosphere, the roughness length is set to 1.5×10^{-4} m, which is a typical value for the ocean surface. In this first approach, the thermal effects have been neglected. It is worth noting that satellite and WRF data sampling is not the same. WRF provides 6-hourly climatological fields while satellite data is not regularly spaced in time. Consequently, the statistical analysis was performed considering all simultaneous and valid wind speed records among the WRF, satellite and buoy databases.

The performance of the model and satellite data in replicating the observed wind conditions is summarized in Table 3. The verification statistics are presented as annual mean values and can be interpreted straightforwardly. In brief, the positive bias suggests the overestimation of the observed wind intensity by the multiple satellites at the selected offshore regions. Conversely, the model underestimates the wind speed magnitude at the corresponding grid points nearest to the buoys locations. Taking into consideration the absolute value of the correlation coefficient, it is concluded that there is a strong degree of linear relationship between measurements, simulations and satellite retrievals though the results suggest a better performance of the latter. Regardless, the high magnitude of RMSE reflects the need for improvement in consistency of the WRF model projections.

A monthly evaluation was also performed by plotting the monthly mean wind speed time-series and evaluating the individual errors in each month. Observing Figure 2 it is possible to conclude that in terms of mean error (bias), the discrepancy between WRF and satellite data is higher from June to November.

It is interesting to notice that WRF underestimates the wind intensity for the greatest part of the year while, in general, satellite data overestimates its magnitude. For satellite winds, the mean bias is lower during the spring and summer seasons and has a tendency to increase during the cold seasons. The underestimation occurring in June and August is less obvious in this case. In contrast, for WRF, major deficiencies in the mean bias are noticeable throughout all year, regardless of the season.

Examining RMSE of satellite wind data reveals that annual errors remain nearly constant throughout time, enhancing the consistent performance of this source of data. WRF has a more random behavior with RMSE denoting an oscillatory pattern, attaining the lowest absolute errors from April to June. Regardless, in terms of this parameter, no particular seasonal trends are noted.

Table 3. Statistical evaluation of wind simulations in coastal waters.

Dataset	bias	RMSE	r	MAE
WRF	–0.15	2.40	0.81	1.81
Satellite	0.25	1.43	0.93	1.05

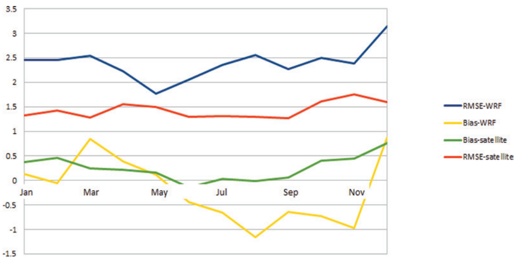

Figure 2. Monthly mean bias and RMSE of WRF and satellite data).

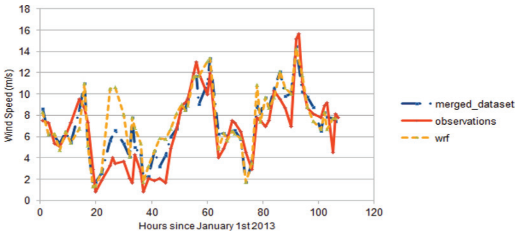

Figure 3. Wind speed time series of WRF (dashed line), blended winds (dash-doted line) and buoy data (solid line).

3.2 *Blended dataset*

The preparation of a blending product has numerous advantages within the context of wind energy assessment. Satellite data is more precise but lacks the spatial and temporal coverage needed for the correct choice of the locations within a project site. In its turn, energy model predictions can be uncertain due to scaling, physical options and deficiencies on the input and boundary data. For that reason, the potential benefit of creating a blended product taking advantage of the strengths of the two wind sources is investigated. Figure 3 provides a short overview of the improvements that can be obtained when using the satellite estimates combined with the WRF data. For the purpose of facilitating the visualization, only a small data sample is depicted in the graphic.

Figure 3 shows the buoy, WRF, and satellite wind speed time series at Cabo Silleiro for a short period of January, 2013. The merged sample was produced using the methodology described in Zgang et al., (2006). Overall, the bias is reduced from 0.80 m/s when considering WRF alone to 0.44 m/s for the blended dataset. The correlation coefficient increases from 0.74 to 0.90 and the RMSE is reduced by more than 15%. The difference may not seem large but as the power density is proportional to the cube of the velocity, small differences in the wind speed precision can have a significant impact in the accuracy of the energy estimates.

4 WIND POWER DENSITY

The main purpose of this paper is to provide valuable information of the energy resources along the Portuguese coastal area. For this purpose, the wind power density (WPD) is calculated over the entire computational grid and further in detail over the north, center and southern regions along the Portuguese coast. The wind power density was calculated considering the wind speed frequency of occurrence in 1 m/s intervals, using the following expression:

$$WPD = \frac{1}{2}\rho V^3 \tag{6}$$

where the air density ρ (kg/m³) is taken as 1.225 kg/m³.

Seven wind power classes are defined according to Oh et al. (2012). For reference, it is worth mentioning that class 3 and above is considered suitable for most wind power projects. This corresponds to a WPD of 150/200 W/m² at 10 m height or the equivalent 5.1/5.6 m/s mean wind speed.

The average wind power density at the height of 10 m for the year of 2013 is represented in Figure 4. As expected, WRF compares reasonably well with satellite observations in most offshore regions. In a general manner, the entire coast has favorable conditions for the exploitation of renewable energy, with WPD exceeding 200 W/m² on a yearly basis. The power flux is higher is the northern regions, particularly in the northwest corner of Galicia, where the average wind energy density is above 650 W/m2. The least energetic areas are mostly located in the south.

Consequently, the pre-feasibility and prospecting stages should be dealt with care in these regions since the mean WPD is close to the 200 W/m² threshold that guarantees profitability. Still, the equipment specifications and amount of time the wind turbine is operating have to be determined to account for factors such as the operating limits, design assumptions and maintenance operations.

4.1 *Wind power density: Case studies*

The implications of using different data sources in estimating the energy density of a potential site can be examined in detail by considering eight proposed locations along the Portuguese coast for building offshore wind parks. The choice was based on a preliminary inspection of the limitations imposed by physical and environmental constraints such as distance to shore, biodiversity protection, shipping routes, military areas, human activity, oil and gas exploration and tourist zones. Once again, the mean WPD is calculated and mapped.

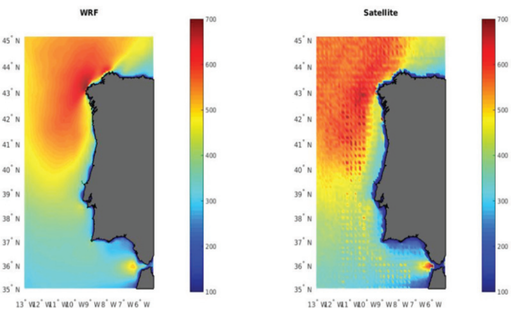

Figure 4. Wind power density calculated using winds obtained from WRF and Multi-Satellite estimates.

4.2 *Case study 1: Southern Portugal: Algarve*

Figures 5 and 6 show two proposed locations for building wind parks in the southern region of Algarve, more specifically offshore the cities of Faro (Area 1) and Albufeira (Area 2). Correspondingly, Table 4 summarizes the mean values of the wind speed and energy density at each proposed location. From observing the maps depicted below, it is concluded that despite the small discrepancy in the average wind speed, differences up to 100 W/m² are found for the energy density, depending on the location inspected. In fact, according to WRF wind data, 277–312 W/m² are available on a yearly basis at the two proposed sites. From satellite wind estimates, only 226 W/m² and 190 W/m² are accessible

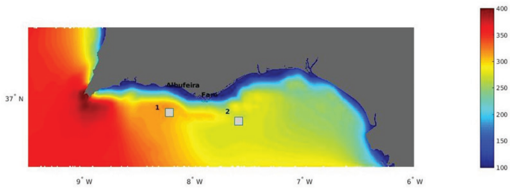

Figure 5. Wind power density for southern Portugal calculated using winds obtained from WRF.

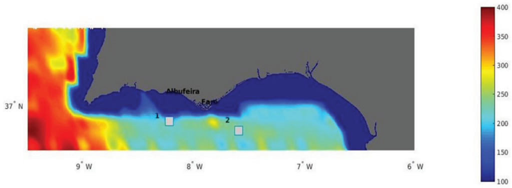

Figure 6. Wind power density for southern Portugal calculated from multi-satellite wind data.

Table 4. Wind speed and power density values for two selected areas locates in southern Portugal.

Source	Area	Area1	Area2
WRF	Wind Speed (m/s)	6.50	5.98
	WPD (W/m²)	312	277
Satellite	Wind Speed (m/s)	5.88	5.69
	WPD (W/m²)	190	226

at areas 1 and 2 respectively. It is worth noting that while WRF points out Area 2 as the most energetic site, satellite data identifies area 1 as the most feasible region. This prompts for a thorough analysis of the wind trends and an uncertainty analysis of the expected profits and associated financial risks.

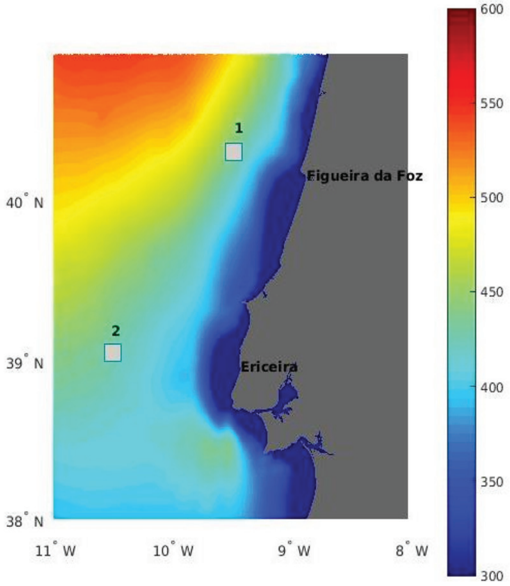

Figure 7. Wind power density for central Portugal calculated using winds obtained from WRF.

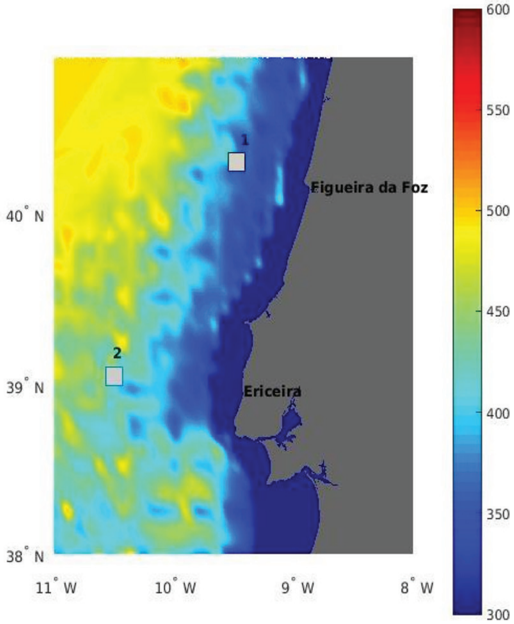

Figure 8. Wind power density for central Portugal calculated from multi-satellite wind data.

4.3 *Case study 2: Central Portugal*

Taking a look at Center Portugal, (Figures 7 and 8) the two proposed areas exhibit a mean wind power density in the 372–442 W/m^2 range according to satellite wind measurements. In reverse, 428–431 W/m^2 are estimated when using WRF model data (Table 5).

Nevertheless, for this case, both datasets suggest area 2 as the one associated to higher energetic potential, despite a small difference in the estimated mean value.

4.4 *Case study 3: Northern Portugal*

For northern Portugal (Figures 9 and 10), WRF projections estimate between 476 and 490 W/m^2 of energy available for extraction. In a similar manner, satellite data indicates a 308–396 W/m^2 power density coverage for the regions offshore Porto, Viana do Castelo and Póvoa do Varzim (Table 6). Area 3 is pointed out as the most energetic, probably

Table 5. Wind speed and power density values for two selected areas located at the centre of Portugal.

Source	Area	Area1	Area2
WRF	Wind Speed (m/s)	7.4	7.58
	WPD (W/m^2)	428	431
Satellite	Wind Speed (m/s)	6.99	7.75
	WPD (W/m^2)	372	442

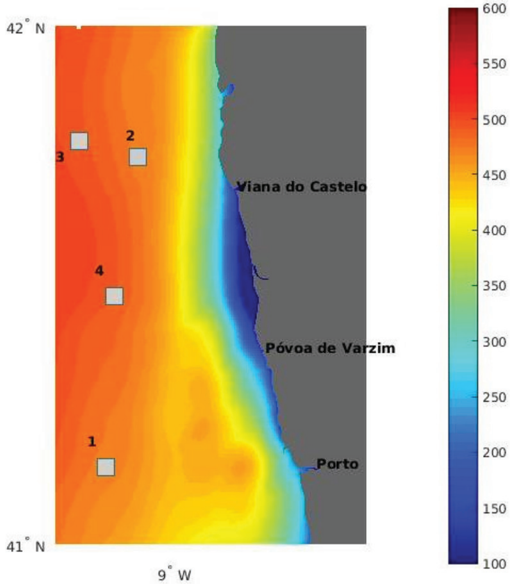

Figure 9. Wind power density for northern Portugal calculated using winds obtained from WRF.

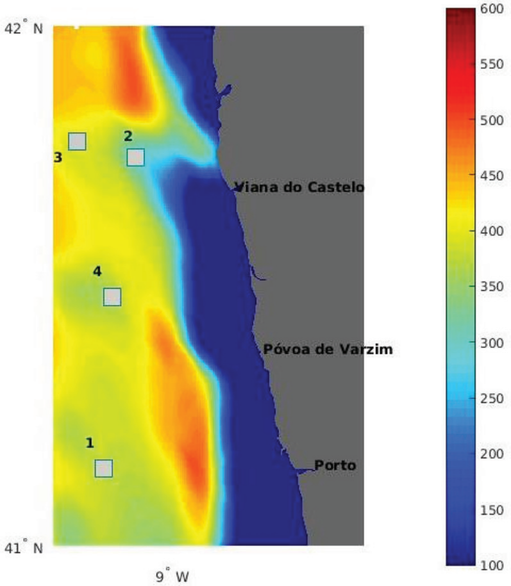

Figure 10. Wind power density for northern Portugal calculated from multi-satellite wind data.

Table 6. Wind speed and power density values for two selected areas located in the north of Portugal.

Source	Area	Area1	Area2	Area3	Area4
WRF	Wind Speed (m/s)	7.67	7.73	7.83	7.73
	WPD (W/m^2)	476	476	490	483
Satellite	Wind Speed (m/s)	7.11	7.05	7.18	6.97
	WPD (W/m^2)	382	308	396	363

due to the greater distance to the coast. Regardless, WRF estimates nearly 100 W/m^2 of additional wind power for the same location, when compared with satellite data projections.

5 CONCLUSIONS

The wind energy available offshore the Portuguese coast obtained from model and satellite data is compared and analyzed in detail. In a general manner, both data sources are well correlated with the measured values, with satellite data surpassing WRF in terms of skillfulness as the statistical values indicate. Despite the discrepancies found, a quick examination of the potential benefit of combining the two sources of wind data shows that satellite data can be complementary to the numerical models, improving the spatial and temporal characteristics of the wind database. In its turn, observations from marine buoys allow for adjustment, correction and validation of the two sources of data.

Analyzing the energy projections for the year of 2013, it can be concluded that the most energetic regions are mostly located in the north and center coasts though there is still a considerable amount of exploitable energy in the southern regions. However, the numbers obtained must be dealt with care since significant differences in the mean projections are obtained when using different sources of data. The results presented in this paper provide guidance for future research on many areas of offshore wind development, with particular focus on the Portuguese coastal region.

ACKNOWLEDGEMENTS

This study was performed within the project ARCWIND – Adaptation and implementation of floating wind energy conversion technology for the Atlantic region, which is co-financed by the European Regional Development Fund through the Interreg Atlantic Area Programme under contract EAPA 344/2016.

REFERENCES

Campos, R. & Guedes Soares C. 2017. Assessment of Three Wind Reanalysis in the North Atlantic Ocean. *Journal of Operational Oceanography*. 10(1):30–44.

Cardinali, C, Zagar, N, Radnoti G, and Buizza R. 2014. Representing model error in ensemble data assimilation. *Nonlinear Processes in Geophysics*, 21(5):971–985.

Castro-Santos, L., Martins, E., and Guedes Soares, C. 2016. Cost assessment methodology for combined wind and wave floating offshore renewable energy systems. *Renewable Energy.* 97:866–880.

Chang, R., Zhu, R., Badger, M., Hasager, C.B, Xing, X. and Jiang, Y. 2015. Offshore Wind Resources Assessment from Multiple Satellite Data and WRF Modeling over South China Sea. *Remote Sens.* 7, 467–487.

European Commission, 2015. Communication from the Commission on *A Framework Strategy for a Resilient Energy Union with a Forward-Looking Climate Change Policy*;

Guo, Q., Xu, X., Zhang, K., Li, Z., Huang, W., Mansaray, L.R., Liu, W., Wang, X., Gao, J., & Huang, J. 2018. Assessing Global Ocean Wind Energy Resources Using Multiple Satellite Data. *Remote Sensing,* 10, 100.

Hasager C., Mouche A., Badger M., Bingöl F., Karagali I., Driesenaar T., Stoffelen A., Peña A., Longépé N. 2015. Offshore wind climatology based on synergetic use of En-visat ASAR, ASCAT and QuikSCAT. *Remote Sensing of Environment,* 156, 247–263.

Hölbig C.A., Machado V.L., Pavan W. 2016. Statistical Correction of the Result of Weather Forecast by Applying the Model Output Calibration. Electronic Notes in Theoretical Computer Science. 324, 79–90.

Lee M.E., Kim G., Jeong S.-T., Ko D.H., Kang K.S., 2013. Assessment of offshore wind energy at Younggwang in Korea. *Renewable and Sustainable Energy Reviews*, 21, 131–141.

Martin R., Lazakis I., Barbouchi S., Johanning L. 2016. Sensitivity analysis of offshore wind farm operation and maintenance cost and availability. *Renewable Energy,* 85, 1226–1236.

Mattar C., Borvarán D. 2016. Offshore wind power simulation by using WRF in the central coast of Chile, *Renewable Energy*, 94, 22–31.

Moosavi, A.S., Rao, V., & Sandu, A. 2018. A Learning Based Approach for Uncertainty Analysis in Numerical Weather Prediction Models. CoRR, abs/1802.08055.

Oh K.Y., Kim J.Y., Lee J.S. 2012. Ryu K.W. Wind resource assessment around Korean Peninsula for feasibility study on 100 MW class offshore wind farm. *Renewable Energy,* 42, 217–226.

Salvação, N. & Guedes Soares, C. 2016. Resource assessment methods in the offshore wind energy sector. L. Castro-Santos & V. Diaz-Casas (Eds.). *Floating Offshore Wind Farms*. Springer International Publishing Switzerland; 121–141.

Salvação, N.; Guedes Soares, C., & Bentamy, A. 2015. Offshore Wind energy assessment for the Iberian coasts using remotely sensed data. Guedes Soares, C. (Ed.). *Renewable Energies Offshore,* London, UK: Taylor & Francis Group 237–244.

Salvação N., & Guedes Soares C. 2018. Wind resource assessment offshore the Atlantic Iberian coast with the WRF model, *Energy,* 145, 276–287.

Salvação N., Bernardino M. and Guedes Soares C. 2014. Assessing mesoscale wind simulations in different environments. *Computers & Geosciences*, 71, 28–36.

Soler-Bientz R., Watson S., Infield D. 2010. Wind characteristics on the Yucatán Peninsula based on short-term data from meteorological stations, *Energy Conversion and Management*, 51, 754–764.

Stolpe, M., Buhl, T., Sumer, B.M., Kiil, S., Holbøll, J., and Piirainen, K. 2014. Offshore wind energy developments. In H.H. Larsen, & L. Sønderberg Petersen (Eds.), *DTU International Energy Report 2014:* Wind energy — drivers and barriers for higher shares of wind in the global power generation mix. Technical University of Denmark (DTU).

Wang, W., Bruyère, C., Duda, M., Dudhia, J., Gill, D., Kavulich, M., Keene, K., Chen, M., Lin, H.-C., Michalakes, J., Rizvi, S., Zhang, X., Berner, J., Ha, S. and Fossel, K. 2018. WRF-*ARW Version 3 Modeling System User's Guide. Mesoscale and Microscale Meteorology Laboratory* – National Center for Atmospheric Research (MMM-NCAR).

Wei, X., Duan, Y., Liu, Y., 2018. Onshore-offshore wind energy resource evaluation based on synergetic use of multiple satellite data and meteorological stations in Jiangsu Province, China; *Frontiers of Earth Science*, pp 1–19.

Zhang, H.-M., Reynolds R.W., and Bates J.G. 2006. Blended and gridded high resolution global sea surface wind speed and climatology from multiple satellites: 1987–present. *14th Conference on Satellite Meteorology and Oceanography,* Atlanta, GA, American Meteorological Society, Paper 100004.